Cellular Interaction and Toxicity Depend on Physicochemical Properties and Surface Modification of Redox-Active Nanomaterials

Janet M. Dowding,[†,∥] Soumen Das,[‡,∥] Amit Kumar,[‡] Talib Dosani,[†] Rameech McCormack,[‡] Ankur Gupta,[‡] Thi X. T. Sayle,[§] Dean C. Sayle,[§] Laurence von Kalm,[⊥] Sudipta Seal,[‡,*] and William T. Self[†,*]

[†]Burnett School of Biomedical Science, College of Medicine, University of Central Florida, Orlando, Florida 32816, United States, [‡]Advance Material Processing Analysis Center and Nanoscience Technology Center, University of Central Florida, Orlando, Florida 32826, United States, [§]School of Physical Sciences, University of Kent, Canterbury CT2 7NZ, United Kingdom, and [⊥]Department of Biology, College of Science, University of Central Florida, Orlando, Florida 32816, United States. [∥]These authors contributed equally to this work.

ABSTRACT The study of the chemical and biological properties of CeO_2 nanoparticles (CNPs) has expanded recently due to its therapeutic potential, and the methods used to synthesize these materials are diverse. Moreover, conflicting reports exist regarding the toxicity of CNPs. To help resolve these discrepancies, we must first determine whether CNPs made by different methods are similar or different in their physicochemical and catalytic properties. In this paper, we have synthesized several forms of CNPs using identical precursors through a wet chemical process but using different oxidizer/reducer; H_2O_2 (CNP1), NH_4OH (CNP2), or hexamethylenetetramine (HMT-CNP1). Physicochemical properties of these CNPs were extensively studied and found to be different depending on the preparation methods. Unlike CNP1 and CNP2, HMT-CNP1 was readily taken into endothelial cells and the aggregation can be visualized using light microscopy. Exposure to HMT-CNP1 also reduced cell viability at a 10-fold lower concentration than CNP1 or CNP2. Surprisingly, exposure to HMT-CNP1 led to substantial decreases in ATP levels. Mechanistic studies revealed that HMT-CNP1 exhibited substantial ATPase (phosphatase) activity. Though CNP2 also exhibits ATPase activity, CNP1 lacked ATPase activity. The difference in catalytic (ATPase) activity of different CNPs preparation may be due to differences in their morphology and oxygen extraction energy. These results suggest that the combination of increased uptake and ATPase activity of HMT-CNP1 may underlie the biomechanism of the toxicity of this preparation of CNPs and may suggest that ATPase activity should be considered when synthesizing CNPs for use in biomedical applications.

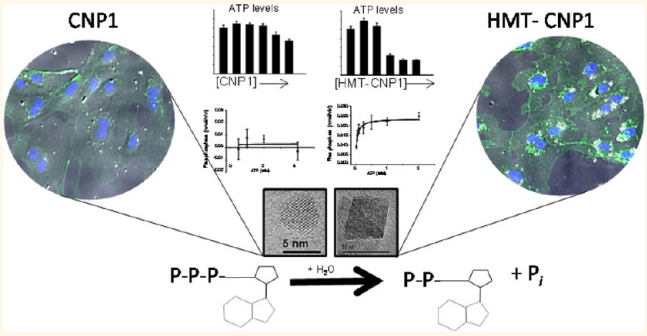

KEYWORDS: cerium oxide nanoparticles · phosphatase activity · toxicity · surface modification · nanoparticle–cell interaction

Cerium is a rare earth metal that belongs to the lanthanides series of the periodic table, and its derivatives are used in many industrial applications.[1] Cerium in its oxide form has a fluorite structure. However, in the nanoscale regime, CeO_2 NPs (CNPs) retain their fluorite structure with oxygen deficiencies, yielding CeO_{2-x}, with vacancies as the most likely sites for reduction–oxidation (redox) reactions.[2] This unique property of CNPs makes them useful for industrial applications including the removal of carbon monoxide (CO), hydrocarbons, and nitric oxide species (NO_x) from exhaust gas.[3] This property of CNPs is facilitated by the ability of CNPs to mediate its oxidation state between 3+ and 4+. The redox potential of CNPs favors the cycling of cerium to scavenge a variety of reactive oxygen species (ROS) and reactive nitrogen species (RNS).[4–7] Moreover, at the same time, the unique oxygen buffering capacity of CNPs allows the regeneration of its trivalent oxidation state (for further scavenging of radicals) without entering into deleterious side reactions for regeneration. The unique regenerative ability to scavenge ROS/RNS species has led to CNPs testing as potential therapeutics in numerous biological systems to reduce potentially harmful ROS/RNS in

* Address correspondence to william.self@ucf.edu, sudipta.seal@ucf.edu.

Received for review December 19, 2012 and accepted May 13, 2013.

Published online May 13, 2013
10.1021/nn305872d

disease and aging. These studies include the protection of biological tissues against radiation-induced damage,[8] prevention against laser-induced retinal damage,[9] induction of angiogenesis through modulation of oxygen,[10] reduction of spinal injury,[11] reduction of chronic inflammation,[12] and control or reduction of the growth and proliferation of tumors and inhibition of the tumorstroma interactions.[12,13]

Nanoparticles in general exhibit novel surface properties and chemistry that influence their interaction with biological systems. For CNPs to be a realistic therapeutic, they must undergo a careful materials and biological characterization in order to ensure safety. Part of that understanding must include a variety of synthesis processes in which the CNPs have been created. The methods used in preparation of CNPs are widely varied;[14] this includes creating NPs with the core CeO_2 nanomaterial with different size, shape, surface modification, and stability of the nanoparticle modifications.[14,15] Even when synthesizing "bare" CNPs, there are numerous synthesis methods that have been employed.[14,16−18] Over the past decades, synthesis methods for use of CNPs have been extensively tested for industrial[19] and biological uses.[20] These methods include hydrolysis, precipitation, thermal deposition, combustion or flame synthesis, sol−gel, hydrothermal, or solvothermal, microemulsion method, gas condensation, sonochemical synthesis, and electrochemical synthesis among others.[14] Several preparation processes and surface coatings have been reported for CNPs for increasing biocompatibility, decreased nonspecific interaction, and stabilization in biological media.[21] Catalytic properties of room temperature/wet chemical synthesis of CNPs have been well studied.[4−7] The rationale for this synthesis method is that they seem to be less toxic[22−24] and there is the ability to control the Ce^{3+}/Ce^{4+} ratio.[25] On the other hand, hexamethylenetetramine (HMT)-based synthesis of CNPs is also routinely employed, and several reports exist on toxicological properties of this preparation both *in vitro* and *in vivo*. However, physicochemical and catalytic properties of HMT-based synthesis of CeO_2 NPs[26−29] were not studied as extensively. Indeed, for CNPs to be a potential therapy for the reduction of ROS/RNS in disease, the mechanism of action for CNPs, respective of synthesis procedure, must be well-defined. Unfortunately, the material synthesis of these studies varies significantly. Thus it must first be determined whether CNPs made by different methods are similar or different in their physicochemical properties. Therefore, the next step is to determine the pathways that CNPs might antagonize or augment based on their synthesis. The underlying mechanisms of antioxidant or pro-oxidant properties of CNPs are now being determined by several groups. However, the outcomes of CNP exposure can vary as much as the synthesis methods and cell types tested.[30−32] This underscores the need to fully understand the nanoparticles' physicochemical properties from different synthesis methods, possibly resulting in different catalytic behavior(s) and their influence(s) in various biological settings (from toxicity to therapeutics). Compared to other non-redox-active nanoparticles, synthesis procedures of CNPs (redox-active) need to be well-controlled to ensure consistency since catalytic/chemical properties of CNPs from varying synthesis procedures may result in catalytically inactive or pro-oxidant CNPs due to potential changes in the surface chemistry of the CNPs. Other than the CNPs' antioxidant property, CNPs also exhibit phosphatase-like activity,[33] yet this activity is poorly understood and its biological relevance is not well understood.

Phosphorylation and dephosphorylation play a significant role in a wide range of important regulatory mechanisms in mammals. Control of the addition or removal of phosphate (PO_4^{3-}) groups is especially important for energy maintenance and is particularly critical for adenosine triphosphate (ATP), which is a critical energy storage molecule. The hydrolysis of ATP to adenosine diphosphate (ADP) releases energy (H^+) and inorganic phosphate which is then utilized in a wide range of cellular applications such as the movement of organelles (endosomes, lysosomes, mitochondria) along microtubules as well as muscle contractions, small molecule transport, or biosynthetic reactions driving anabolism. Any perturbation of ATP levels can have a significant effect on cellular physiology and metabolism, yet the ability of redox-active nanomaterials to alter ATP levels has rarely been carried out in previous studies.

In this study, we compared CNPs synthesized using wet chemical methods varying the oxidizer/reductant (H_2O_2, NH_4OH precipitation, and HMT-based) to begin to understand the enigma of how CNPs can be reported to be both toxic and nontoxic when exposed to a variety of organisms and cells in culture at similar concentrations. On the basis of our results, the toxicity of HMT-CNPs may be due to differential cellular uptake and dissimilar catalytic properties of CNPs that proceeds through a poorly understood catalytic mechanism at the surface of the nanoparticle.

RESULTS AND DISCUSSION

CNPs Vary in Size, Shape, Surface Charge, and Physicochemical Properties Depending upon the Synthesis Method. Careful characterization of nanoparticle preparations used in a study is critical when addressing catalytic properties and biological relevance. In this study, we chose different synthesis procedures for making CNPs and varying the physicochemical properties. These methods have been frequently used in the literature since it has been established that biological properties vary depending upon the synthesis method.[15] CNPs

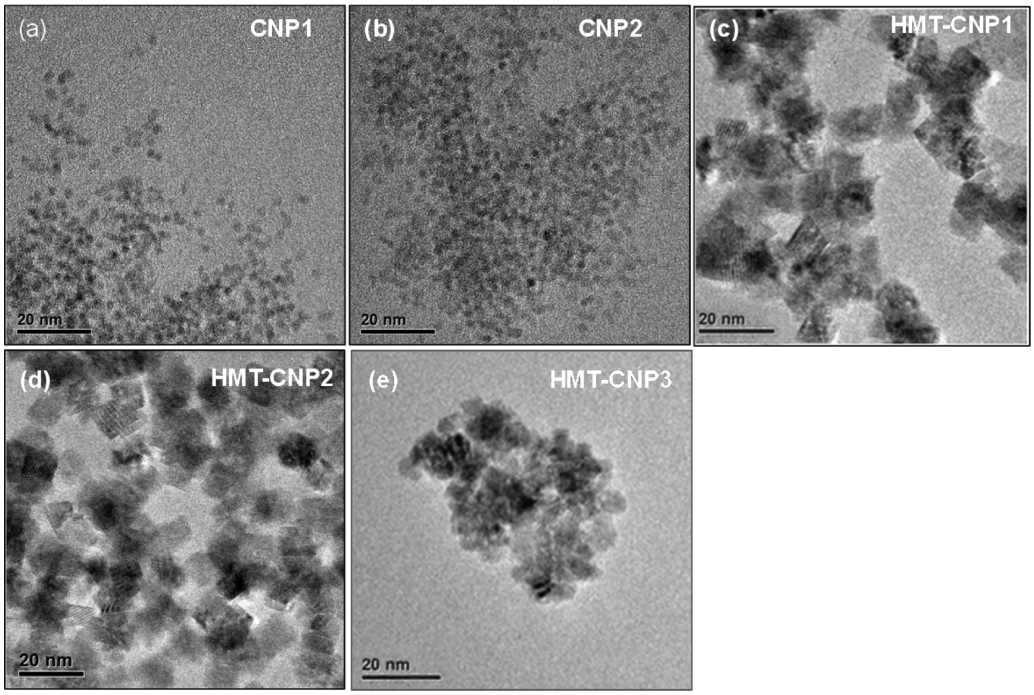

Figure 1. Size, shape, and morphology variation of cerium oxide nanoparticles (CNP). TEM images of CNPs prepared using water-based (a,b) or solvent HMT (c−e) synthesis methods. (a) CNP1. (b) CNP2. (c) HMT-CNP1. (d) HMT-CNP2. (e) HMT-CNP3.

prepared using H_2O_2 (CNP1), NH_4OH (CNP2), or hexamethylenetetramine (HMT) (HMT-CNP1) were characterized thoroughly. We modified the HMT preparation method to produce nanoparticles with varying amounts of HMT on the surface and to generate a spherical morphology. HMT-CNP2 (higher levels of HMT) was produced by omitting the acetone wash during the final washing stages. A spherical morphology of cerium oxide nanoparticles (HMT-CNP3) was produced by preheating the precursor solution. High-resolution transmission electron microscopy (HRTEM) images of all of the nanoparticles are shown in Figure 1 ((a) CNP1, (b) CNP2, (c) HMT-CNP1, (d)-HMT-CNP2, and (e) HMT-CNP3). Selected area diffraction pattern (SEAD) confirmed the crystalline property of all of the nanoparticles (Supplementary Figure S1). In general, CNP1 and CNP2 are smaller and rounder than the HMT-CNPs which display a sharp, angular shape. This demonstrates that depending upon the synthesis method and the differing conditions during synthesis (see Materials and Methods) nanoparticles of the same cerium oxide composition (CeO_2) can be very different morphologically yet the biological relevance of these differences is poorly understood.

CNPs in general exhibit novel surface properties, and change in nanoparticle morphology and surface properties due to different synthesis conditions, media, and process can affect their interaction with biological systems. Table 1 contains a chart outlining the physicochemical characteristics of all CNPs used throughout this study. The details of the synthesis are described in the Materials and Methods section. Distribution of the hydrodynamic radius of individual particles is shown in Supplementary Figure S2a−e. Surface charge differences of CNPs (CNP1 and CNP2) and HMT-CNPs were also estimated in dH_2O suspension. Additionally, Supplementary Table S1 contains data of the size and zeta-potential of the various CNPs when in culture media for 4 or 24 h. CNPs dispersed in culture media showed a slight increase in size as compared to water and zeta-potential values changed from positive to slightly negative. The surface oxidation state (Ce^{3+}/Ce^{4+} ratio) of the CNP preparations was calculated from X-ray photoelectron spectroscopy (XPS) data as described previously.[34] The intensity of peaks at 880.8, 885.8, 899.3, and 903.5 eV corresponding to the cerium(III) oxidation state and intensity of peaks at 881.9, 888.4, 897.9, 901.2, 906.8, and 916.3 eV corresponding to the cerium(IV) were determined and ratios calculated. Deconvoluted XPS spectra for all nanoparticles used in this study are shown in Supplementary Figure S3a−e. Fourier transform infrared (FTIR) spectra of HMT and HMT-CNP1 revealed residual HMT on the surface of the HMT-CNP1 as compared with CNP1 (Supplementary Figure S4). The level of the organic was determined to contain HMT and was estimated by calculating differential scanning calorimetry thermogravimetric analysis (DSC-TGA) by the percentage of weight loss.[35] TGA plots of thermal decomposition of HMT present on the surface of the HMT-CNPs are shown in Supplementary Figure S5a−c, which confirmed the amount of HMT/organic contaminate on the surface of the nanoparticles.

TABLE 1. Physicochemical Properties of Cerium Oxide Nanoparticles (CNPs) Prepared by Water-Based or HMT-Based Method

particle characteristics	CNP1	CNP2	HMT-CNP1	HMT-CNP2	HMT-CNP3
morphology	round	round	polygonal	polygonal	round
crystalline property	crystalline fluorite structure	crystalline fluorite structure	crystalline fluorite structure	crystalline fluorite structure	crystalline fluorite structure
size (TEM) (nm)	3−5	5−8	10−15	10−15	8−10
hydrodynamic radii (nm)	30.84 ± 2.8	69.26 ± 4.5	147.70 ± 6.4	83.56 ± 3.2	129.20 ± 4.1
zeta-potential (mV)	18.6 ± 0.6	30.2 ± 1.5	34.6 ± 1.7	38.6 ± 2.3	36.7 ± 2.1
hexamethyltetramine (wt %)			1.68 ± 0.2	8.16 ± 0.7	1.78 ± 0.3
surface Ce^{3+}/Ce^{4+} ratio	1.28	0.37	0.37	0.36	0.32
BET (m^2/g)	92	102	86	71	118

Moreover, XPS spectra of nitrogen 1s (N 1s) of HMT-CNP1 also confirm the presence of HMT on the surface of the nanoparticles. Interestingly, a shift in peak position of N 1s was observed for HMT-CNP1 (399.05 eV) compared to pure HMT (399.15 eV) (Supplementary Figure S6). The shift in peak position may be due to an interaction of HMT nitrogen with surface of the CNP1.

CNP1 and CNP2 were crystalline, and due to their nanometer length scale, oxygen defects at the surface are present that yield reactive sites.[1] Within these sites, CNPs have the ability to interchange between 3+ and 4+ oxidation states.[5] Two different CNPs exhibiting mixed Ce^{3+}/Ce^{4+} valence states were synthesized.[25] CNPs with a higher 3+/4+ ratio of approximately 1.28 (CNP1) exhibit efficient superoxide dismutase (SOD) activity[5,6] when compared to CeO_2 NPs with lower 3+/4+ ratio of approximately 0.37 (CNP2). It should be noted that CeO_2 NPs with a lower 3+/4+ ratio (CNP2) exhibit increased catalase mimetic activity[7] as well as the ability to effectively scavenge soluble nitric oxide (•NO).[4] HMT-based CNPs (HMT-CNP1, HMT-CNP2, or HMT-CNP3) contained lower 3+/4+ ratios measuring 0.37, 0.36, and 0.32, respectively, very similar to CNP2, however, without having any catalytic natures toward superoxide, hydrogen peroxide, or •NO (Supplementary Figure S15a−e). HMT-CNP1 and HMT-CNP3 as synthesized contained very similar concentrations of HMT, 1.68 and 1.78% HMT, respectively; however, they differ in their shape with HMT-CNP1 morphology as polygonal and HMT-CNP3 morphology as round (Figure 1). HMT-CNP1 (1.68%) differed from HMT-CNP2 (8.16%) in the amount of HMT present on the surface of the nanoparticles. In addition, the mean hydrodynamic ratios of all three HMT-CNPs were increased when compared to that of CNP1 or CNP2.

Nanoparticles have high surface area to volume ratios, and the physical properties of a nanoparticle can be dominated by the nature of the nanoparticle surface.[36] Particle size and surface area are important features when considering *in vivo* nano-bio reactivity.[37] High surface areas can also increase surface reactivity leading to catalytic activities that can be both beneficial and detrimental to cells.[15] The surface areas, as determined by BET, closely ranged between 71 and 118 m^2/g, and it appeared that the presence of HMT had no dramatic influence on surface area.

HMT-Based Nanoparticles Are More Toxic than CNP1 or CNP2. The rapid development of CNPs for various potential applications in the field of nanomedicine has led to numerous studies evaluating CNP toxicity or biocompatibility. We employed the primary cell type human umbilical vein endothelial cells (HUVECs) as a biological model to test toxicity in the context of human tissue. To investigate whether different particles made using different synthesis methods can effect overt toxicity, HUVEC cells were exposed to increasing CNP concentrations (0, 0.02, 0.08, 0.86, 8.6, 17 μg/mL) for 48 h (Figure 2). It should be noted that the HMT-CNPs were extensively washed during synthesis to avoid adsorption of background molecules of HMT onto the NPs to prevent the residual HMT from affecting the NPs' surface chemistry or be present in the aqueous portion of the samples (see Materials and Methods). We observed a reduced toxicity for CNP1, as previously reported[11] (Figure 2a) with similar observations for CNP2 (Figure 2b). Even at the highest concentrations (17 μg/mL), CNP1 and CNP2 only had modest effects on cell viability (20%) whereas HMT-CNP1 showed a greater reduction in cell viability (30%). However, at a 10-fold lower concentration (0.86 μg/mL), the HMT-CNP1 begin to exhibit a derogatory effect whereas the water-based CNP1 and CNP2 did not (Figure 2c). To address whether the HMT concentration was responsible for the deceased cell viability, HMT-CNP2s which contain 8.16% HMT (Figure 2d) were also tested, and MTT results are similar to HMT-CNP1 (Figure 2c).

Sharp edges and corners present in the nanoparticle crystal structure may cause mechanical damage to the cell membrane which might also play a role in mediating toxicity to cells/living organism.[38] HMT-CNP1 have a polygonal shape and thus sharp edges. Therefore, to address if shape of the nanoparticle was a factor in toxicity, HMT-CNP3 containing similar concentration of HMT as HMT-CNP1, however, having a

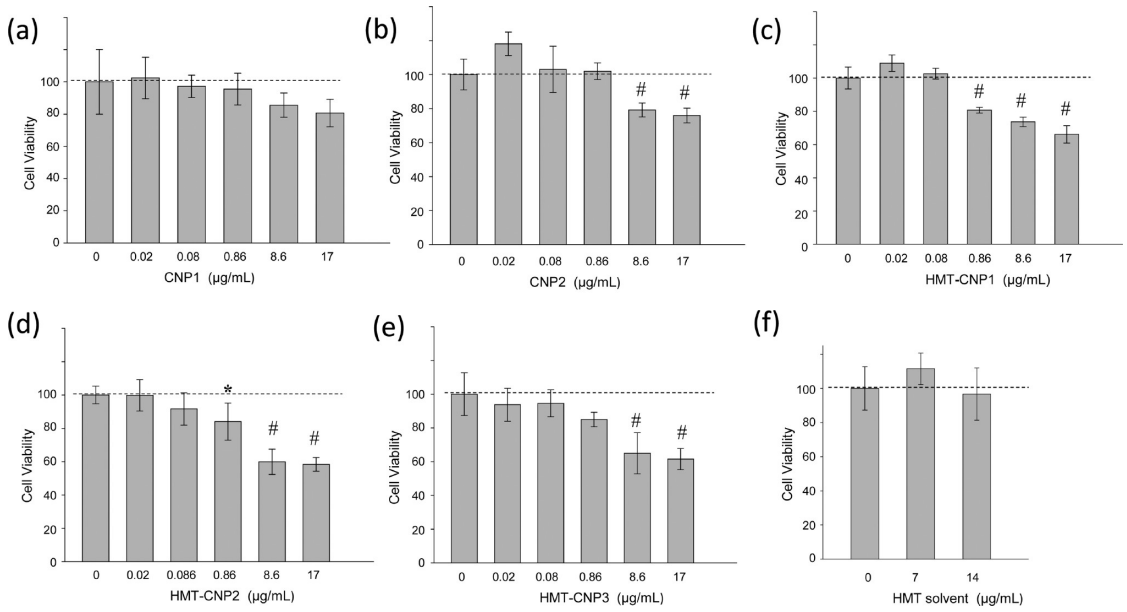

Figure 2. Cell viability of HUVECs exposed to various preparations of CNPs. HUVEC cells were exposed to increasing CNP concentrations (0, 0.02, 0.08, 0.86, 8.6, 17 μg/mL). (a) CNP1. (b) CNP2. (c) HMT-CNP1. (d) HMT-CNP2. (e) HMT-CNP3. Cell viability was determined by dividing the absorbance of treated samples to untreated controls and reported as a percentage of control cells. The mean of at least 4 independent cultures is plotted with standard deviation as error; #, $p \leq 0.001$.

rounder appearance (Figure 1e), similar to CNP1 and CNP2 (Figure 1a,b), were tested. MTT results for HMT-CNP3 (Figure 2e) were again similar to HMT-CNP1, strongly suggesting that increasing HMT concentration or shape did not play a role in the decreased HUVEC viability of HMT-CNP1 when compared to CNP1 and CNP2. Additionally, all three HMT-CNPs started to show decreased cell viability at 0.86 μg/mL concentration, whereas neither CNP1 or CNP2 exhibited any toxicity at the 0.86 μg/mL concentration. To rule out that decreased cell viability was due solely to the presence of the HMT solvent, we tested the higher concentrations of HMT solvent only and found no toxicity to be attributed to the presence of the solvent alone (Figure 2f). The MTT assay relies upon metabolically active cells to reduce the MTT dye. The cell's source of energy is supplied by adenosine-5′-triphosphate (ATP) and is produced in mitochondria (*via* oxidative phosphorylation) or by glycolysis (which takes place in the cytoplasm). HUVECs are a primary cell line that primarily uses oxidative phosphorylation to acquire its energy. This led us to determine if intercellular ATP levels of HUVECs exposed to various preparations of CNPs were affected.

Exposure to HMT-CNP Leads to Decreases in Intercellular ATP Levels. To determine a possible mechanism linking exposure to HMT-CNPs and reduced HUVEC viability, we treated HUVECs with increasing CNP concentrations (0, 0.02, 0.08, 0.86, 8.6, 17 μg/mL) and measured ATP levels in cell lysates at 48 h as an alternative to MTT reduction. At the higher exposure concentrations (17 μg/mL), both CNP1 (Figure 3a) and CNP2 (Figure 3b) had diminished ATP levels (70−68%, respectively) as compared to controls. However, HMT-CNP1-treated cells showed dramatically reduced ATP levels at a 20-fold lower exposure of 0.86 μg/mL (42%, Figure 3c). We found similar decreases at the 0.86 μg/mL concentrations using HMT-CNP2 (Figure 3d) and HMT-CNP3 (Figure 3e). Similar to our MTT results, HMT solvent alone had no effect on ATP concentration (Figure 3f). Thus exposure to HMT-CNPs at lower doses resulted in a significant reduction in ATP levels than CNP1 or CNP2 exposure.

HMT-CNP1s Aggregate in Exposed HUVEC Cells. CNPs are readily internalized by cells due to their small size. Since the HMT-CNPs all had similar toxicities (Figures 2 and 3) as well as phosphatase activities (to be discussed later in paper (Supplementary Figure S11c)), we chose to use HMT-CNP1 for additional in-depth comparisons with CNP1 and CNP2. Untreated HUVECs as well as CNP1- and CNP2-treated (8.6 μg/mL) HUVECs exhibited no visible morphological changes (Figure 4a−c). Strikingly, HUVECs treated with HMT-CNP1 at the same concentration exhibited visible changes in morphology with live-cell imaging using a 40× objective (Figure 4d). The ability to see nanoparticles using unaided microscopy techniques is uncommon. In the study by Yokel *et al.*, similar CeO_2 NP agglomerations were seen in light microscope images of spleen of rats treated with 250 mg/kg CeO_2 NPs after only 1 h.[39] These intracellular accumulations led us to probe further the biological interaction of our CeO_2 NPs with HUVECs.

Confocal Laser Scanning Microscopy (CLSM) Images Reveal Perinuclear Aggregation of HMT-CNP in HUVECs. It has been reported that CNPs dispersed directly into culture media may form aggregates after internalization into

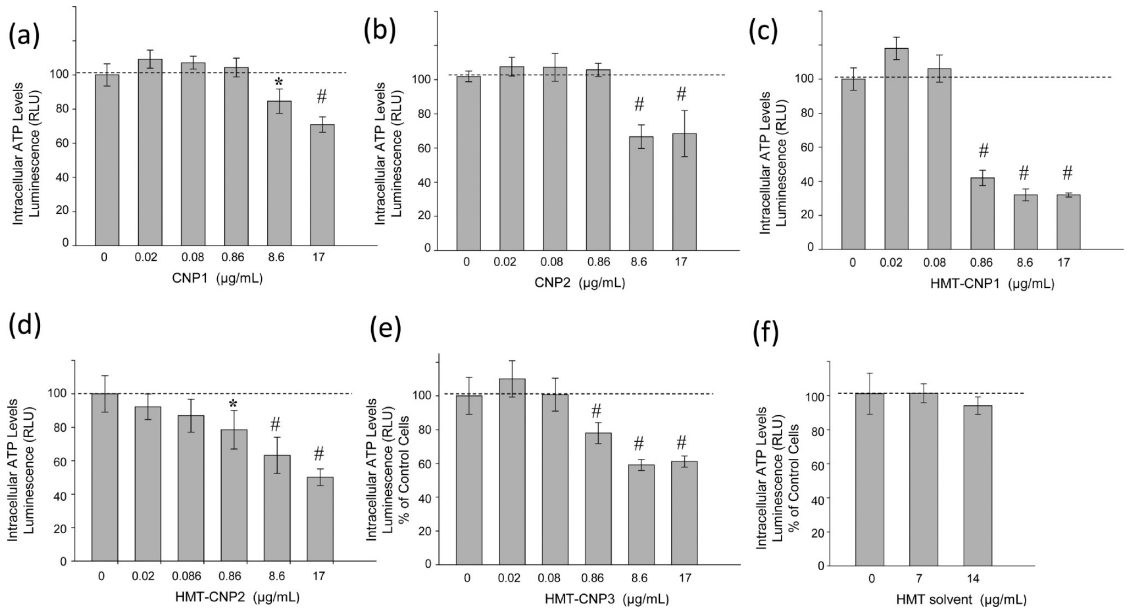

Figure 3. Intercellular ATP levels of HUVECs exposed to various preparations of CNPs. HUVEC cells were exposed to increasing CNP concentrations (0.02, 0.08, 0.86, 8.6 17 μg/mL). (a) CNP1. (b) CNP2. (c) HMT-CNP1. (d) HMT-CNP2. (e) HMT-CNP3. ATP level was determined by dividing the luminescence of treated samples to untreated controls and reported as a percentage of control cells. The mean of at least 4 independent cultures is plotted with standard deviation as error; *, $p \leq 0.05$, #, $p \leq 0.001$.

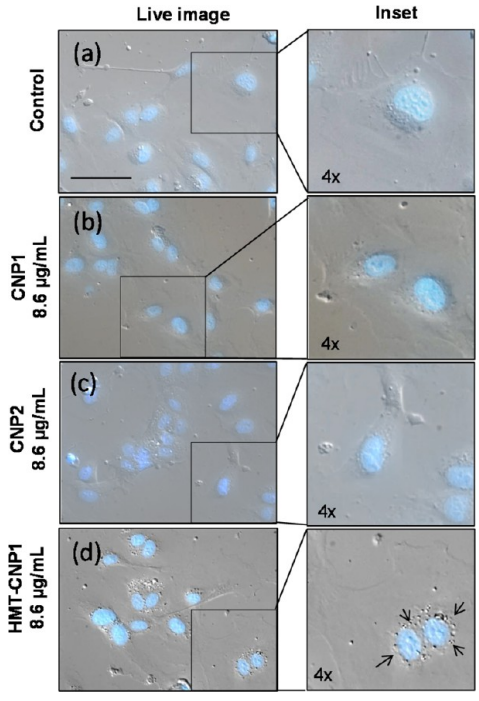

Figure 4. Live-cell examination of HUVEC cells exposed to HMT-CNP1. HUVEC cells were exposed to 8.6 μg/mL CNPs for 20 h. (a) Control cells. (b) CNP1. (c) CNP2. (d) HMT-CNP1. Hoescht dye was added just before imaging to show location of nuclei. Representative images feature 4$\times$ zoom of region of interest. Scale bar = 50 μm.

cells.[40] To confirm whether the dense granules visualized by bright-field microscopy were actually HMT-CNP1 aggregates within the cell and not simply associated outside the cells, HUVECs were treated for 24 h with nanoparticles, washed repeatedly, trypsinized, and seeded onto glass coverslips for 4 h (to allow for cell attachment) before fixation. Using immunocytochemistry, we labeled the plasma membranes of HUVECs with wheat germ agglutinin (WGA) with fluorescein conjugate and took simultaneous fluorescent and bright-field imaging using confocal microscopy. Untreated, CNP1- and CNP2-treated HUVECs (8.6 μg/mL) under bright-field and merged channels show no evidence of nanoparticle aggregation (Figure 5a,b). By contrast, HUVECs treated with HMT-CNP1 (8.6 μg/mL) showed a robust increase in agglomerated, granular material in both the bright-field and merged channels (Figure 5d). This aggregation becomes even more evident in HUVECs treated with a higher concentration of HMT-CNP1 (86 μg/mL) (Supplementary Figure S7), and at this concentration, the nuclei are condensed, indicating that cells are dying or dead after only 24 h of treatment. Cell death is corroborated by MTT and ATP assays using the 86 μg/mL concentration (Supplemental Figure S8a,d). Notably, CLSM strongly suggested that the apparent dense granules were in fact intracellular HMT-CNP1s and their subcellular location was perinuclear. The subcellular localization is in agreement with previous studies testing CNPs using *in vitro* cell culture models.[41] To explore the toxicity and drop in ATP concentrations by HMT-CNP1 further, we considered that the intercellular location of the HMT-CNP1 may play a role in their toxic nature. The wheat germ agglutinin antibody used in Figure 5 and Supplementary Figure S7 specifically labels glycoproteins in plasma membranes as well the ER and Golgi—the location in the cells where sugars are incorporated

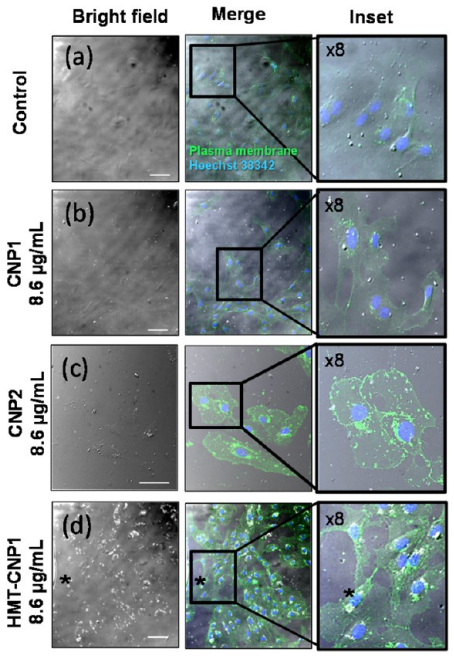

Figure 5. Intracellular aggregation of HMT-CNP1 as viewed by confocal laser scanning microscopy (CLSM). Cells were exposed to nanoparticles for 24 h, washed, trypsinized, and seeded onto glass coverslips for 4 h (to allow for attachment), fixed, and labeled with antibody for identification of plasma membranes (green channel) and Hoechst 33342 (blue channel) for identification of nuclei. (a) Control/no treatment; (b) 8.6 μg/mL CNP1; (c) 8.6 μg/mL CNP2; (d) 8.6 μg/mL HMT-CNP1. Scale bar = 50 μM. Asterisk follows representative region of HMT-CNP1 aggregation.

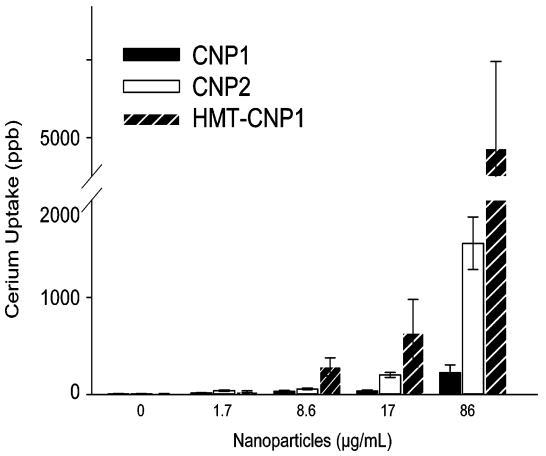

Figure 6. Increased uptake of HMT-CNP1 as measured by ICP-MS. HUVEC cells were incubated with various CNPs for 24 h, washed two times to remove extracellular nanoparticles, collected by trypsination, and washed with PBS again to remove excess media and particles which may be adsorbed on the surface of the cells. The concentration of cerium inside cells was measured by ICP-MS as described in Materials and Methods.

into proteins in cells—in all cell images. We found the HMT-CNP1 aggregated in a perinuclear location, aligning with the endoplasmic reticulum (ER) as visualized by WGA antibody. To further establish intercellular localization and in order to better visualize the HMT-CNP1, a fluorescent probe was conjugated to the HMT-CNP1 (FL-HMT-CNP1), and their subcellular localization was determined with respect to mitochondria and lysosomes (Supplementary Figure S9). FL-HMT-CNP1-treated HUVEC cells were labeled with Mitotracker. It did not appear that FL-HMT-CNP1 colocalize with mitochondria based on the merged image (Supplementary Figure S9b), suggesting the drop in ATP levels was not necessarily due to a direct interaction with mitochondria or proteins present in the electron transport chain including ATPases. Nanoparticles as well as most macromolecules are taken up in cells by the endosomal/lysosomal pathway. To determine if FL-HMT-CNP1 colocalized with lysosomes, HUVEC cells were labeled with Lysotracker and a portion of the FL-HMT-CNP1 was found to colocalize with lysosomes (Supplementary Figure S9c). Together, these confocal studies demonstrate that the HMT-CNP1/FL-HMT-CNP1 appear to be located in the perinuclear region, aligning with the ER and colocalizing mainly with lysosomes. Though the FL-HMT-CNP1 did not colocalize with mitochondria, mitochondria and ER are intimately connected and both play an essential role in cellular Ca^{2+} homeostasis.[42] It is possible that a portion of the toxicity and drop in ATP concentrations is due to the aggregation of HMT-CNP1 and their cellular location, yet the decreases in ATP levels are likely due to the observed phosphatase activity given the localization of the particles.

HMT-CNP1 Are Transported into HUVECs More Efficiently than Water-Based Cerium Oxide Nanoparticles. Uptake of nanomaterial varies vastly between materials tested and cell types.[43,44] On the basis of the morphological changes in HUVECs treated with HMT-CNP1 easily seen by light microscopy, we incubated HUVECs with increasing concentrations (0, 1.7, 8.6, 17, 86 μg/mL) of CNP1, CNP2, and HMT-CNP1 and harvested cells after 24 h. We used inductively coupled plasma mass spectrometry (ICP-MS) to determine the concentration of cerium inside the cells. Interestingly, CNP2 uptake was more efficient than CNP1 uptake, and cellular uptake of HMT-CNP1 was greatly increased in HUVECs at every concentration tested (Figure 6). Detection of NPs at a concentration of 1.7 μg/mL by ICP-MS was nominal, but our biological data (Figures 2 and 3) clearly demonstrate that there is an effect in cell viability and ATP concentrations at 0.86 μg/mL for HMT-CNP1. This discrepancy may be due to the detectable limit of ICP-MS. When comparing the ATP levels, MTT assay data (Figures 2, 3, and Supplementary Figure S8), and the uptake analysis, it is clear that exposure to relatively low levels of HMT-CNP impacts energy metabolism. If ATP hydrolysis is indeed occurring, the mitochondrial enzyme activity is possibly tryng to compensate in order to maintain sufficient ATP for cellular function. This likely explains why the

MTT assay and ATP levels are not in complete agreement when assumed to reflect cell viability. Furthermore, this is precisely why we followed the NPs using multiple methods in terms of subcellular localization (Figures 4, 5, and Supplementary Figure S9). The zeta-potentials of CNP1, CNP2, and HMT-CNP1 were very similar (∼−10) (Supplementary Table S1); therefore, surface charge is not likely a major influence on the interaction of the particles with the cells. Thus, the HMT contamination on the surface of the HMT-CNP1 might play an important role in increased cellular internalization as compared to CNP2 and CNP1. Taken together, this clearly shows that HMT-CNP1s are readily internalized by HUVEC cells, and this could be a contributing factor as to the toxicity previously observed in a *Caenorhabditis elegans* model[29] as well as their exhibiting an oxidant-induced change in gene expression effect in a mouse neuronal model.[45] We tested CNP1 and HMT-CNP1 in a comparable model system, *Drosophila melanogaster*, and found that CNP1s were not toxic and HMT-CNP1 NPs were only marginally toxic at a concentration of 86 μg/mL (Supplementary Figure S10) when fed to larvae. Though it is not practical to test the catalytic activity or size distribution in the fly food, the nanoparticles were sonicated prior to addition to the food and particle size gradient distribution[46] allows for many sized particles and minimizes possible agglomeration effect of particles, preventing uptake by the feeding larvae. However, these effects, if present, would be shared equally between all samples tested. Thus, uptake must be taken under consideration when determining toxicity as well as inherent differences in model systems, in our case *in vitro* cell culture toxicity *versus* whole animal marginal toxicity. Our ICP-MS data show CNP2 are also readily taken up by HUVEC cells compared to CNP1, especially at higher concentrations, and yet they have not shown toxicity when compared to HMT-CNP1 in HUVECs. It should be noted that CNP2 exhibits catalase mimetic activity and scavenge •NO,[4,7] and therefore, these catalytic activities could be at the basis for their lack of toxicity.[47]

CNPs with Increased Surface 4+ Character Exhibit Phosphatase and ATPase Activity. Phosphorylation and dephosphorylation play significant roles in cell signaling, energy transfer, and utilization within cells. Phosphate ester hydrolysis of biological molecules by CNPs would have important implications in their potential toxicity. In order to test any potential phosphatase activity of CNPs and HMT-CNPs, we first used *p*-nitrophenyl phosphate (pNPP) as a screening substrate.[33] This assay uses an artificial chromogenic substrate that is readily hydrolyzed by phosphatases and allowed us to detect any potential phosphatase mimetic activity. We found that CNP2 as well as HMT-CNP1 were able to dephosphorylate pNPP, whereas CNP1 did not (Supplementary Figure S11a). These results agreed with previous observations for CNPs,[33] and our initial results strongly suggested that CNPs with increased 4+ shared a similar catalytic activity. In order to corroborate the phosphatase mimetic activity and possibly explain the mechanism of cell death, we used ATP as the substrate and looked at free phosphate production using two different assays. Our results show again that CNP1 did not act as a phosphatase using ATP for the substrate (Supplementary Figure S12). SiO_2 NPs, a metal oxide NP of similar size, were used as a negative control and also did not cause the release of phosphate (Supplementary Figure S11a−c). However, CNP2 and HMT-CNP1 did release phosphate from ATP, with CNP2 showing a robust activity (Supplementary Figure 11b). To obtain quantitative information on the effect of CNP2 and HMT-CNP1, we determined the apparent K_m. Experimentally, we followed the kinetics of P_i released in a continuous reaction and determined the initial rates of free phosphate release from 34 μg/mL NPs in the presence of increasing concentrations of ATP (Figure 7a−d). The apparent K_m for HMT-CNP1 was 39.9 ± 8.2 μM. CNP2s were efficient phosphatases at lower substrate concentrations; however, when approaching physicological concentrations of ATP, CNP2s reached saturation and rates declined (Figure 7a). The CNP2 apparent K_m was determined to be 48.4 ± 10.6 μM. We compared the kinetic behavior of CNPs with an established, physiologically relevant ATPase, dynein ATPase, which has a reported K_m of 20 μM.[48] We chose to compare to a motor protein since they have multiple active sites,[49] which is similar to nanoparticles having numerous oxygen vacancies for reactions to occur. In addition, dynein ATPase is located in the cytoplasm, along the same location as we saw the aggregation of HMT-CNP1 NPs (Figures 4 and 5). However, CNPs differ from dynein ATPase in terms of turnover rate. Dynein APTase V_{max} is 0.22 μM/s;[48] however, the V_{max} values for CNP1 and HMT-CNP1 were 0.017 and 0.024 nmol/min, respectively.

Finally, to simulate the potential phosphatase activity of CNPs in cell culture, we measured pNPP hydrolysis in the presence of increasing amounts of fetal bovine serum (FBS). Nanoparticles in cells come into contact with various proteins and other molecules potentially forming a corona which is dynamic and is affected by particle material, size, and surface properties.[50] In some cases, the corona may lead to newly acquired nanoparticle properties.[37] Supplementary Figure S13 clearly demonstrates that CNP2 phosphatase activity diminishes with increasing concentrations of FBS, whereas HMT-CNP1 phosphatase activity was not affected, even in the presence of up to 10% FBS. Collectively, these results suggest that CNPs with increased level of 4+, regardless of their synthesis method, are competent phosphatases. They were able to hydrolyze various substrates including pNPP

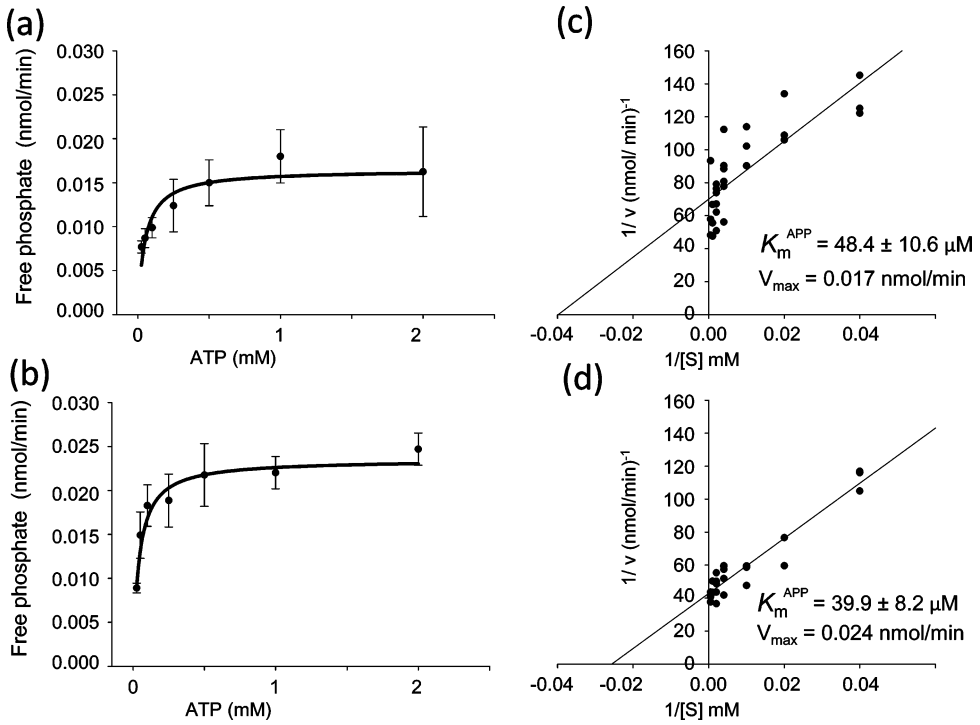

Figure 7. CNP2 and HMT-CNP1s exhibit significant ATPase activity at physiologically relevant concentrations of ATP. ATPase activity of CNPs was quantified by measuring phosphate released with EnzCheck phosphate assay using varying concentrations of ATP with 34 μg/mL NPs. (a) CNP2. (b) HMT-CNP1. Line plot is representative of 3 or more experiments. Double reciprocal plots of ATPase activity with ATP as substrate using constant concentration of NPs (34 μg/mL). (c) CNP2. (d) HMT-CNP1.

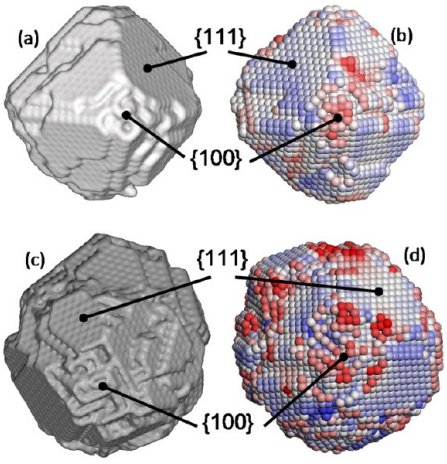

Figure 8. Atomistic models of CNPs. (a) Surface rendered model of a CNP with polyhedral morphology; (b) reactivity fingerprint of the polyhedral CNP; (c) surface rendered model of a CNP with "spherical" morphology; (d) reactivity fingerprint of the spherical CNP.

(Supplementary Figure S11a,c), ATP (Supplementary Figure S11b and Figure 7), and GTP (data not shown). Furthermore, shape (HMT-CNP2) and increased HMT concentration on the surface (HMT-CNP3) were able to similarly hydrolyze ATP when compared to HMT-CNP1 (Supplemental Figure S11c). However, HMT-CNP1 is more readily taken up by cells, so the concentration of the catalyst in cells is higher than those exposed to CNP2. Additionally, the difference in phosphatase activity might be due to decreased surface area of the HMT-CNP1 (10−12 nm) as compared to CNP2 (3−5 nm) as well as HMT-CNP1's phosphatase activity is not affected by increasing concentrations of FBS. This suggests that the protein−HMT nanoparticle corona appears to be less detrimental to their phosphatase activity as compared to the protein−CNP2 corona, leading to a decreased level of CNP2 phosphatase activity. Presence of HMT molecules on the surface of the nanoparticles may also interfere with the interaction of ATP with the CNP surface, which may also be one of the causes of decreased phosphatase activity of HMT-CNP1 as compared to CNP2. Further, to find out if oxygen vacancy on the surface of the nanoparticles may play a role in phosphatase activity, we estimated the oxygen vacancies using Raman spectroscopy. Differences in surface oxygen vacancies of HMT-CNP1 and CNP2 were observed (Supplementary Figure S14). In particular, both CNP2 and HMT-CNP1 have similar Ce^{3+}/Ce^{4+} oxidation state ratios; however, the oxygen vacancy of CNP2 was found to be $2.49 \pm 0.13 \times 10^{21}$ and $3.59 \pm 0.25 \times 10^{21}$ for HMT-CNP2. Micro ceria were included as references, and vacancy calculation showed less oxygen vacancy (1.16×10^{21}) as compared to nano-sized particles. Therefore, decreasing oxygen vacancies might also play a role in increasing the phosphatase activity of the nanoparticles. This can be explained by Scheme 1. Possible correlation of oxygen vacancy with catalytic property of the nanoparticles

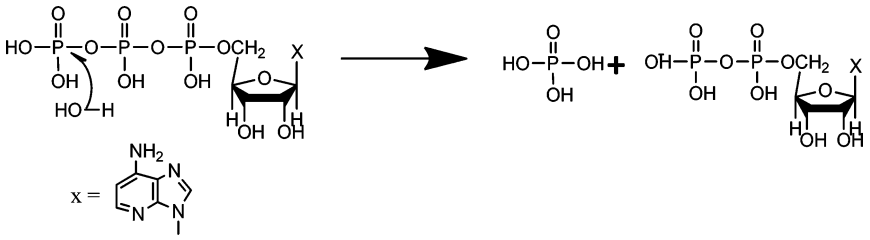

Scheme 1

TABLE 2. Synthesis Method Determines Surface Character and Catalytic Activities of CNPs[a]

catalytic activity	assay	CNP1	CNP2	HMT-CNP1	SiO_2
phosphatase	pNPP	no	yes	yes	no
ATPase	malachite green	no	yes	yes	no
	ENZCheck	no	yes	yes	n/d[b]
•NO scavenger	CuFl assay	no[4]	yes[4]	no	no[4]
catalase mimetic	UV−visible	no[7]	yes[7]	no	no
SOD mimetic	cytochrome *c*	yes[6]	no[6]	no	no

[a] Various properties of CNPs have been tested for their ability to exhibit SOD mimetic,[6] catalase mimetic,[7] •NO scavenging,[4] phosphatase, or ATPase activities. [b] Not determined.

might be explained in terms of water dissociation and availability of the −OH group on the surface of the nanoparticles. Oxygen vacancy strongly coordinates with the −OH group and decreased the availability of −OH on the surface[51], which in turn decreases the phosphatase activity of the nanoparticles.

Synthesis Method Determines Surface Catalytic Character of CNPs. Having identified ATPase as a critical catalytic character for HMT-CNPs in terms of toxicity, we tested these preparations of CNPs to assess the effect of synthesis on their catalytic activity at a broader level. To evaluate the potential catalytic activities, we tested HMT-CNP1s for their ability to scavenge •NO or to act as SOD or catalase mimetics. Unlike CNP1 or CNP2, HMT-CNP1s did not show any reactivity toward •NO (Supplementary Figure S15a,b), superoxide (Supplementary Figure S15c), and hydrogen peroxide (Supplementary Figure S15d,e).

Reduction of Ce^{4+} to Ce^{3+} causes oxygen vacancies or defects on the surface of the crystalline lattice structure of the particles, generating a cage for redox reactions to occur.[52] It has been established that the specificity of some of the catalytic activities depend upon the ratio of Ce^{3+}/Ce^{4+}.[4,53] Table 2 highlights how the wet chemical synthesis method of CNPs without HMT leads to unique physical and chemical/catalytic characteristics that are not found in CNPs synthesized by the HMT-based method. In addition, these catalytic activities seem to correlate with the 3+/4+ ratio, specifically NPs with more Ce^{4+} displaying phosphatase activity. This reiterates the need for the careful characterization of nanoparticle preparations and a thorough understanding of their catalytic activities. These findings support previous publications showing toxicity of HMT-CNP-based CeO_2 NPs.[29,45]

Correlation of Nanoparticle Morphology with Reactivity. To help understand and interpret the different catalytic activities of CNP2 and HMT-CNP1 (both having similar Ce^{3+}/Ce^{4+} ratio), molecular dynamics (MD) simulation was used to generate full atomistic models of CNPs with different morphologies. The models were then used to interrogate their surface activity to enable a morphology−activity correlation. This information will help reveal whether the morphology of CNP can influence their chemical activity—specifically how the morphology might influence the ease of liberating oxygen from the surface of the nanoparticle.

Experimental fabrication of CNPs typically involves a crystallization step during synthesis. Simulated amorphization and crystallization was used to generate full atomistic models for CNPs. The atomistic structures of two CNPs, with different morphologies, are shown in Figure 8. The first nanoparticle (Figure 8a,b) exhibits a polyhedral morphology and exposes predominantly {111} surfaces together with a small amount of {100}. Conversely, the second CNP (Figure 8c,d) appears more spherical and exposes at the surface a greater proportion of {100} compared to {111} surfaces. The nanoparticle with polyhedral morphology (Figure 8a,b) is therefore a model representative of HMT-CNP1, and the pseudospherical nanoparticle (Figure 8c,d) is a model representative of CNP2.

A comparison between the calculated activity "fingerprints" (Figure 8b,d) for the polyhedral (HMT-CNP1) and spherical morphologies (CNP2), respectively, reveals that the "spherical" morphology/CNP2 (Figure 8d) is more active toward surface oxygen release compared to the CNP with polyhedral morphology/HMT-CNP1 (Figure 8b), which further supports our experimental, catalase, and phosphatase activity observations of CNP2 and HMT-CNP1. In particular, the {111} surfaces are predicted to be less active toward oxygen release from the surface compared to {100} surfaces. The simulations therefore predict that the morphology of CNPs can influence significantly their surface activity—specifically their ability to liberate oxygen from the surface.

CONCLUSION

The toxicology and surface reactivity of CeO_2 nanoparticles synthesized by wet chemical method using

different oxidizing/reducing agents were compared in this work in order to elucidate the mechanisms behind the varied observations with biological models in the current literature. In this study, we showed that HMT-CNP1s are readily taken up by HUVECs (Figure 6) and their aggregation was visible using conventional light microscopy techniques (Figures 4 and 5). An increase in the uptake of HMT-CNP1 certainly could have a negative effect on a HUVEC cell's metabolism along with their perinuclear aggregation. Compared to CNP2, enhanced cellular internalization of HMT-CNP1 may indicate that residual surface HMT promotes cellular interaction and internalization of CNPs. However, the CNP2s are also taken up but do not aggregate (Figures 5 and 6), and the internalization is approximately one-third as compared to HMT-CNP. The reduced, relative toxicity by CNP2 may be explained in terms of lower cellular internalization as compared to HMT-CNP1 (Figure 6) as well as CNP2s are catalase mimetics[7] and scavenge soluble •NO.[4]

Herein, we have demonstrated that synthesis methods of CNPs can affect surface properties. For non-redox-active nanoparticles, varying the synthesis procedure may not have a substantial effect, but our data demonstrate that it is not the case when dealing with redox-active nanomaterials. A slight change in physicochemical properties (Table 1) can give you a vast difference in the redox properties of the nanomaterials (Table 2). Kuchma *et al.* report that the phosphatase activity appears to be dependent upon the cerium(III) sites.[33] It is possible that the ATPase activity seen in the CNP2 and HMT-CNP1 may be due to a nucleophile attraction of the Ce^{3+} and the terminal phosphate on an ATP molecule. Paradoxically, CNP1s, which have more vacancies on the surface, are not phosphatase mimetics. Moreover, simulation results reveled that morphology also has an influence on nanoparticle reactivity, which may explain the lower phosphatase activity of HMT-CNP1 as compared to CNP2, while they have similar Ce^{3+}/Ce^{4+} ratios on the surface. Moreover, higher oxygen vacancy/decreased availability of −OH on the surface of HMT-CNP1 potentially makes them less reactive toward phosphatase activity.

Although most of the focus of CeO_2 NP research has been on the ability of these materials to reduce reactive oxygen and nitrogen species in biological systems,[54] there are reports that claim that nanoceria are toxic. Unfortunately, the material synthesis methods used are not always clearly reported, and it is likely that these observed toxicities are due to different physicochemical properties and unwanted surface modification. The CNPs synthesized in HMT resulted in different surface chemistry, which resulted in different catalytic activities than the CNPs synthesized without HMT. The increased uptake and phosphatase/ATPase activity of HMT-CNP1 may underlie their toxicity. With the recent burgeoning growth of the use of CNPs as potential therapeutics, synthesis method and surface chemistries must be emphasized.

MATERIALS AND METHODS

Preparation of Different Cerium Oxide Nanoparticles. In this study, several CNPs were prepared with varying surface oxidation state, surface modification, and morphology. Cerium nitrate hexahydrate (99.999% pure from Sigma Aldrich, St. Louis, MO) was used as a precursor for all of the preparations. Cerium oxide nanoparticles with a higher Ce^{3+}/Ce^{4+} ratio (CNP1) or with lower Ce^{3+}/Ce^{4+} ratio (CNP2) were prepared using a wet chemical method as described previously.[55] Briefly, precursor dissolved in distilled water (dH_2O) and stoichiometric H_2O_2 (CNP1) or NH_4OH (CNP2) was added to the precursor solution. After addition of H_2O_2 (CNP1) or NH_4OH (CNP2), solutions were mixed properly. NH_4OH preparation was washed four times with ddH_2O and resuspended in the same volume of water. The pH of both nanoparticles' suspensions was then adjusted to 3 to get stable suspensions. Surface-modified cerium oxide nanoparticles were prepared using hexamethylenetetramine.[56] Briefly, equal volumes of 37.5 mM cerium nitrate solution and 0.5 M HMT were mixed together and stirred for 24 h at room temperature. Cerium oxide nanoparticles prepared using HMT were washed with either ethanol and acetone or dH_2O three times and finally resuspended in dH_2O. It is important to mention that, after washing with ethanol and acetone, CNP-HMT1 was washed with dH_2O (three times) to remove any trace amount of solvent (ethanol or acetone) before resuspending in dH_2O. Cerium oxide nanoparticles washed with ethanol and acetone to remove the maximum amount of HMT were designated as HMT-CNP1. CNPs washed with only dH_2O were designated as HMT-CNP2. Different morphologies of HMT-CNP3 were prepared by preheating both the solutions (37.5 mM cerium nitrate precursor and 0.5 M HMT) at 60 °C, and then equal volumes of the solutions were mixed and stirred for 4 h. CNPs formed were then washed with ethanol and acetone three times and finally with dH_2O to remove the solvent before resuspending in dH_2O. All of the nanoparticles were aged for the same amount of time (six weeks) before the start of the biological and catalytic experiment. Moreover, all of the nanoparticles were stored at room temperature and in a glass container to ensure similar storage conditions and to minimize any external influence. All of the nanoparticles used in different reactions were characterized thoroughly after six weeks of aging and to ensure stable water-dispersed nanoparticles.

Preparation of Fluorescence-Conjugated HMT-CNP1. HMT ceria was partially coated with (3-amino)propyltrimethoxysilane. A 1:0.1 molar ratio of HMT CeO_2/silane was used for partial coating or amine functionalization, and the reaction was carried out in toluene. Excess silane was removed by washing. Then amine-functionalized HMT-CNP was conjugated to NHS-fluorescein using *N*-(3-dimethylaminopropyl)-*N'*-ethylcarbodiimide (EDC) and *N*-hydroxysuccinimide (NHS) chemistry.[57] Free fluorescence molecules were removed by washing with distilled water.

Physicochemical Properties of Cerium Oxide Nanoparticles (CNP). High-resolution transmission electron microscopy (HRTEM) was used to analyze size and morphology of the nanoparticles. Hydrodynamic radius and surface charge of the nanoparticles were estimated using Zetasizer (Nano-ZS from Malvern Instruments, Houston, TX). X-ray photoelectron spectroscopy (5400 PHI ESCA) was used to determine the surface oxidation state of the nanoparticles. Mg Kα X-ray irradiation (1253.6 eV) and 350 W power were used during the data collection as previously described.[55] Fourier transform infrared (FTIR) spectra were collected to confirm the presence of any HMT molecule on the nanoparticle surface using a PerkinElmer spectrum IR spectrophotometer (Waltham, MA). The amount of HMT that remains on the surface

of the nanoparticles was determined with differential scanning calorimetry and thermogravimetric analysis (DSC-TGA) using a TA Instruments SDT-Q600 (New Castle, DE), with open alumina pans under 100 mL/min air flow. Particle size analysis was also carried out by measuring the specific surface area (m^2/g) using the Brunauer, Emmett, and Teller (BET) method with a Quantachrome Nova 4200e surface area analyzer (Boynton Beach, FL).

Cultivation of HUVECs. Human umbilical vein endothelial cells (HUVECs) (Lonza Walkerville, Inc., Walkersville, MD) were maintained at 37 °C in a humidified atmosphere containing 5% CO_2 in endothelial basal medium (EBM) (Lonza Walkerville, Inc., Walkersville, MD) supplemented with 2% fetal bovine serum (FBS). Only cells from passages 3−6 were used in experiments.

Cell Viability MTT Assay. HUVECs were cultured in 96-well plates and exposed to CNPs for 48 h followed by addition of thiazoyl blue tetrazolium bromide (MTT) (Amresco, Solon, OH) (1.2 mM) as previously described.[58] Cell viability was determined by dividing the absorbance of treated samples to untreated controls and reported as a percentage of control cells. Results were collected from at least three independent experiments and are expressed as mean ± standard deviation (sd). Statistical analysis of two populations was compared using two-tailed nonpaired Student's *t* test.

Analysis of Intracellular ATP Levels. HUVECs were cultured in opaque-walled 96-well plates and treated with CNPs for 48 h. Plates were equilibrated to room temperature, and cells were lysed according to manufacturer's instructions. CellTiter-Glo reagent was added, and plates were incubated for 10 min to stabilize the luminescent signal. Luminescence was then recorded with a Varian Cary Eclipse fluorescence spectrophotometer (Palo Alto, CA) using 1 s integration time per well. Results were collected from at least three or more independent experiments and are expressed as mean ± standard deviation (sd). Statistical analysis of two populations was compared using two-tailed nonpaired Student's *t* test.

ICP-MS Uptake of CNP Studies. HUVEC culture monolayers were incubated for 24 h with nanoparticles. Cells were washed two times to remove extracellular nanoparticles and then collected by trypsination and washed with PBS again to remove excess media and particles that could be adsorbed on the surface of the cells. Cells exposed to CNPs were analyzed for their cerium content using a Thermo Electron X-Series inductively coupled plasma mass spectrometer (ICP-MS, Thermo Scientific, Pittsburgh, PA) following APHA method 3125B to determine the amount of CNPs taken up by the cells.

Live-Cell Imaging of HUVECs Exposed to CNPs. HUVECs were cultured on Lab-TekII chambered coverglass (NUNC, Rochester, NY) slides in phenol red-free EBM (Lonza, Walkersville, MD) supplemented with 2% FBS. Cells were exposed to various preparations of CNPs for 36 h. To visualize nuclei, Hoechst 33342 dye (Molecular Probes, Invitrogen, Eugene, OR) (1 μg/mL) was added to the medium for 10 min at 37 °C in a humidified 5% CO_2 incubator. Dye was removed and replaced with prewarmed medium. Chamber slides with cultured HUVECs were examined under phase-contrast 40× air objective on a Nikon Eclipse Ti fluorescence microscope (model 602542, Melville, NY) and images acquired at 37 °C in a humidified 5% CO_2 atmosphere.

Confocal Microscopy. HUVECs were exposed to nanoparticles for 24 h and subsequently washed, trypsinized, and seeded onto glass coverslips for 4 h (to allow for cell attachment). Cells were then fixed in 4% formaldehyde for 20 min at room temperature. Cells were washed two times in PBS and then labeled with wheat germ agglutinin (WGA), Alexa Fluor 488 (Molecular Probes, Invitrogen, Eugene, OR) (5 μg/mL) for identification of plasma membranes (green channel, excitation 405 nm/emission 498), and Hoechst 33342 for identification of nuclei (blue channel, excitation 405/emission 428). Cells were washed and mounted in antifade mounting media (Calbiochem, St. Louis, MO) and slides cured 24 h at room temperature. Slides were stored at 4 °C until simultaneous confocal and bright-field imaging by Leica TCS SP5 laser scanning confocal microscope (Buffalo Grove, IL) with 40×/1.25 oil objective lens.

Phosphatase Mimetic Assay. To measure the phosphatase activity of various CNPs, 1.2 mM of *p*-nitrophenyl phosphate (pNPP) (New England BioLabs Inc., Ipswich, MA) was incubated in a 96-well plate in the presence of various concentrations of CNPs (4.3, 8.6, 17, 34 μg/mL) in a total volume of 200 μL of H_2O. The ability of CNPs to catalyze the hydrolysis of pNPP to *p*-nitrophenyl was measured by following the increasing absorbance (405 nm) every minute for 20 min using a Spectramax 190 UV−visible spectrophotometer (Molecular Devices, Sunnyvale, CA).

ATPase Activity Assays. The concentration of inorganic phosphate liberated by various preparations of CNPs was determined using a malachite green assay (R&D Systems, Minneapolis, MN). Nanoparticles (34 μg/mL) were added to ATP or GTP (Sigma Aldrich, St. Louis, MO) (34 μg/mL) at various time points (0, 30 s, 1 min, 2 min, 4 min, 6 min, 8 min, 10 min) at room temperature in 50 mM Tris buffer at pH 8.0. A phosphate standard curve was generated to enable quantitative determination of phosphate. The malachite green solutions were added to each well, and the absorbance (620 nm) was determined using a Spectramax 190 UV−visible spectrophotometer (Molecular Devices, Sunnyvale, CA) after a 20 min incubation to stabilize the dye/PO_4 complex.

The concentration of inorganic phosphate liberated by various preparations of CNPs was also determined using the EnzCheck phosphate assay (Invitrogen, Grand Island, NY). The EnzCheck phosphate reaction is a fast, quantitative enzymatically linked assay in which in the presence of P_i the substrate 2-amino-6-mercapto-7-methylpurine riboside (MESG) is converted enzymatically by purine nucleoside phosphorylase (PNP) to ribose 1-phosphate and 2-amino-6-mercapto-7-methyl purine. The conversion of MESG can be followed by the increase in absorbance at 360 nm. Nanoparticles (34 μg/mL) were added to varying concentrations of ATP (Sigma Aldrich, St. Louis, MO), and phosphate release followed every 30 s for 30 min at 360 nm using a Spectramax 190 UV−visible spectrophotometer (Molecular Devices, Sunnyvale, CA) after an initial 10 min incubation. A phosphate standard curve was generated to enable quantitative determination of phosphate in solution. Baseline changes due to hydrolysis of phosphate from ATP only controls was subtracted from each concentration to determine free phosphate liberated only by addition of CNPs. The kinetic parameters, V_{max} and K_m, were calculated by using SigmaPlot 10 software (Systat Software, Inc., Point Richmond, CA).

Drosophila melanogaster Exposure to CNP1, CNP2, or HMT-CNP1 Cerium Oxide Nanoparticles. Male and female wild-type *D. melanogaster* (Oregon R) were maintained under optimal conditions in a standard corn meal medium at a temperature of 25 °C.[59] Exposure to nanoparticles began at the larval stage and continued through eclosion of adults. Parental crosses were set up in cages with 150 females and 30−40 males on grape plates seeded with live yeast. After 21 h, each grape plate was changed and hatched larvae removed. Groups of 50 larvae from grape plates were isolated using a mounting needle under a dissecting microscope and placed in vials containing 6 mL of Jazzmix (Fisher Scientific, Pittsburgh, PA) food medium containing 86 μg/mL of nanoparticles CNP1 or HMT-CNP1. Control larvae were cultured in parallel in food vials containing only H_2O or 500 μM HMT. All vials were kept at 25 °C and checked daily for pupariation and eclosion. Statistical analysis was performed using one-way ANOVA followed by post-hoc Tukey's test using Statistical Packages for the Social Sciences (SPSS) software.

Raman Spectroscopy. Raman spectra were collected using a Horiba JobinYvon LabRam infrared (IR) micro-Raman system using a 633 nm helium−neon laser with a spatial resolution of 2 μm to obtain the electronic structure. Defect concentration of the nanomaterials was calculated using the following equations as described.[60,61]

$$\Gamma\ (\mathrm{cm}^{-1}) = 5 + 5.81/d_g \qquad (1)$$

where Γ and d_g are half width at half-maxima (hwhm) and grain size, respectively.

$$L\ (\mathrm{nm}) = \sqrt[3]{\left(\frac{\alpha}{2d_g}\right)^2}\,[(d_g - 2\alpha)^3 + 4{d_g}^2\alpha] \qquad (2)$$

where L is correlation length (average distance between two lattice defects) and α is radius of CeO_2 units (0.34 nm).

$$N = 3/4\pi L^3 \quad (3)$$

where N is defect concentration.

Simulation. Simulated amorphization and crystallization was used to generate full atomistic models for CNPs. This method has been described in detail previously,[62] and therefore, only the salient details are presented below.

CNPs were cut from the parent bulk material and amorphized/melted by heating under MD simulation to temperatures above the melting point. Once molten, MD simulation was continued at temperatures below the melting point, which enabled crystalline seeds to spontaneously evolve and nucleate the crystallization of the nanoparticle. A structural distribution of model nanoparticles was generated by altering the temperature of the crystallization step. In particular, temperature changes led to differences in morphology and microstructure (such as dislocations, grain boundaries).

Equipped with atomistic models, the surface activities of the CNPs were interrogated by determining the ease of extracting oxygen from the surface of the nanoparticle. We have shown previously that the energy required to extract oxygen from the surface of a CNP correlates with the electrostatic potential of the individual oxygen atoms comprising the nanoparticle[63] enabling visual "activity fingerprints" to be generated. Accordingly, the activity fingerprints were calculated for the CNPs and presented graphically.

Conflict of Interest: The authors declare no competing financial interest.

Acknowledgment. We thank Hoon Park and Dr. Alfons Schulte from UCF Department of Physics for their assistance with Raman spectroscopy. We thank Jeffery Hatcher and Dr. Jack Cheng from UCF Burnett School of Biomedical Science, Department of Medicine for assistance with confocal microscopy. This work is supported by NIH Grant R01AG031529-01 as well as NSF Grant NIRT CBET 0708172. Additional support includes CBET 1028996 (NSF International Supplement) and CBET 0804733 (NSF REU supplement to R.M.). Finally, support from EPSRC: EP/H001220 for funding to D.C.S.

Supporting Information Available: SEAD spectra (Figure S1); hydrodynamic radius (Figure S2); surface chemistry (Figure S3); FTIR spectra of different CNP nanoparticles (Figure S4); DSC-TGA analysis (Figure S5); CLSM images of nanoparticles intracellular aggregation at higher concentration (Figure S7); cell viability and ATP levels at higher concentrations (Figure S8); colocalization images (Figure S9); toxicity profile of CNP on *Drosophila melanogaster* (Figure S10); pNPP and ATP hydrolysis by various preparations of CNPs (Figure S11); ATPase activity of CNP1 (Figure S12); ATPase activity of different CNP nanoparticles in the presence of FBS (Figure S13); Raman spectra of different CNP nanoparticles (Figure S14); catalytic activities of different CNP nanoparticles (Figure S15); hydrodynamic radius in media (Table S1). This material is available free of charge *via* the Internet at http://pubs.acs.org.

REFERENCES AND NOTES

1. Campbell, C. T.; Peden, C. H. Chemistry. Oxygen Vacancies and Catalysis on Ceria Surfaces. *Science* **2005**, *309*, 713–714.
2. Tsai, Y. Y.; Oca-Cossio, J.; Lin, S. M.; Woan, K.; Yu, P. C.; Sigmund, W. Reactive Oxygen Species Scavenging Properties of ZrO_2-CeO_2 Solid Solution Nanoparticles. *Nanomedicine* **2008**, *3*, 637–645.
3. Masui, T.; Ozaki, T.; Machida, K.; Adachi, G. Preparation of Ceria-Zirconia Sub-catalysts for Automotive Exhaust Cleaning. *J. Alloys Compd.* **2000**, *303*, 49–55.
4. Dowding, J. M.; Dosani, T.; Kumar, A.; Seal, S.; Self, W. T. Cerium Oxide Nanoparticles Scavenge Nitric Oxide Radical (•NO). *Chem. Commun.* **2012**, *48*, 4896–4898.
5. Heckert, E. G.; Karakoti, A. S.; Seal, S.; Self, W. T. The Role of Cerium Redox State in the SOD Mimetic Activity of Nanoceria. *Biomaterials* **2008**, *29*, 2705–2709.
6. Korsvik, C.; Patil, S.; Seal, S.; Self, W. T. Superoxide Dismutase Mimetic Properties Exhibited by Vacancy Engineered Ceria Nanoparticles. *Chem. Commun.* **2007**, *0*, 1056–1058.
7. Pirmohamed, T.; Dowding, J. M.; Singh, S.; Wasserman, B.; Heckert, E.; Karakoti, A. S.; King, J. E.; Seal, S.; Self, W. T. Nanoceria Exhibit Redox State-Dependent Catalase Mimetic Activity. *Chem. Commun.* **2010**, *46*, 2736–2738.
8. Tarnuzzer, R. W.; Colon, J.; Patil, S.; Seal, S. Vacancy Engineered Ceria Nanostructures for Protection from Radiation-Induced Cellular Damage. *Nano Lett.* **2005**, *5*, 2573–2577.
9. Chen, J.; Patil, S.; Seal, S.; McGinnis, J. F. Rare Earth Nanoparticles Prevent Retinal Degeneration Induced by Intracellular Peroxides. *Nat. Nanotechnol.* **2006**, *1*, 142–150.
10. Das, S.; Singh, S.; Dowding, J. M.; Oommen, S.; Kumar, A.; Sayle, T. X.; Saraf, S.; Patra, C. R.; Vlahakis, N. E.; Sayle, D. C.; *et al.* The Induction of Angiogenesis by Cerium Oxide Nanoparticles through the Modulation of Oxygen in Intracellular Environments. *Biomaterials* **2012**, *33*, 7746–7755.
11. Das, M.; Patil, S.; Bhargava, N.; Kang, J. F.; Riedel, L. M.; Seal, S.; Hickman, J. J. Auto-catalytic Ceria Nanoparticles Offer Neuroprotection to Adult Rat Spinal Cord Neurons. *Biomaterials* **2007**, *28*, 1918–1925.
12. Hirst, S. M.; Karakoti, A. S.; Tyler, R. D.; Sriranganathan, N.; Seal, S.; Reilly, C. M. Anti-inflammatory Properties of Cerium Oxide Nanoparticles. *Small* **2009**, *5*, 2848–2856.
13. Alili, L.; Sack, M.; Karakoti, A. S.; Teuber, S.; Puschmann, K.; Hirst, S. M.; Reilly, C. M.; Zanger, K.; Stahl, W.; Das, S.; *et al.* Combined Cytotoxic and Anti-invasive Properties of Redox-Active Nanoparticles in Tumor-Stroma Interactions. *Biomaterials* **2011**, *32*, 2918–2929.
14. Sun, C. W.; Li, H.; Chen, L. Q. Nanostructured Ceria-Based Materials: Synthesis, Properties, and Applications. *Energy Environ. Sci.* **2012**, *5*, 8475–8505.
15. Karakoti, A. S.; Munusamy, P.; Hostetler, K.; Kodali, V.; Kuchibhatla, S.; Orr, G.; Pounds, J. G.; Teeguarden, J. G.; Thrall, B. D.; Baer, D. R. Preparation and Characterization Challenges To Understanding Environmental and Biological Impacts of Ceria Nanoparticles. *Surf. Interface Anal.* **2012**, *44*, 882–889.
16. Bumajdad, A.; Eastoe, J.; Mathew, A. Cerium Oxide Nanoparticles Prepared in Self-Assembled Systems. *Adv. Colloid Interface Sci.* **2009**, *147–148*, 56–66.
17. Karakoti, A. S.; Kuchibhatla, S. V. N. T.; Babu, K. S.; Seal, S. Direct Synthesis of Nanoceria in Aqueous Polyhydroxyl Solutions. *J. Phys. Chem. C* **2007**, *111*, 17232–17240.
18. Sathyamurthy, S.; Leonard, K. J.; Dabestani, R. T.; Paranthaman, M. P. Reverse Micellar Synthesis of Cerium Oxide Nanoparticles. *Nanotechnology* **2005**, *16*, 1960–1964.
19. He, H.-W.; Wu, X.-Q.; Ren, W.; Shi, P.; Yao, X.; Song, Z.-T. Synthesis of Crystalline Cerium Dioxide Hydrosol by a Sol–Gel Method. *Ceram. Int.* **2012**, *38*, S501–S504.
20. Celardo, I.; Pedersen, J. Z.; Traversa, E.; Ghibelli, L. Pharmacological Potential of Cerium Oxide Nanoparticles. *Nanoscale* **2011**, *3*, 1411–1420.
21. Karakoti, A. S.; Singh, S.; Kumar, A.; Malinska, M.; Kuchibhatla, S. V. N. T.; Wozniak, K.; Self, W. T.; Seal, S. PEGylated Nanoceria as Radical Scavenger with Tunable Redox Chemistry. *J. Am. Chem. Soc.* **2009**, *131*, 14144–14145.
22. Chen, J.; Patil, S.; Seal, S.; McGinnis, J. F. Rare Earth Nanoparticles Prevent Retinal Degeneration Induced by Intracellular Peroxides. *Nat. Nanotechnol.* **2006**, *1*, 142–50.
23. Hirst, S. M.; Karakoti, A.; Singh, S.; Self, W.; Tyler, R.; Seal, S.; Reilly, C. M. Bio-distribution and *In Vivo* Antioxidant Effects of Cerium Oxide Nanoparticles in Mice. *Environ. Toxicol.* **2011**, *28*, 107–118.
24. Niu, J.; Wang, K.; Kolattukudy, P. E. Cerium Oxide Nanoparticles Inhibit Oxidative Stress and Nuclear Factor-κb Activation in H9c2 Cardiomyocytes Exposed to Cigarette Smoke Extract. *J. Pharmacol. Exp. Ther.* **2011**, *338*, 53–61.
25. Patil, S.; Kuiry, S. C.; Seal, S.; Vanfleet, R. Synthesis of Nanocrystalline Ceria Particles for High Temperature Oxidation Resistant Coating. *J. Nanopart. Res.* **2002**, *4*, 433–438.

26. Zhou, X. D.; Huebner, W.; Anderson, H. U. Processing of Nanometer-Scale CeO_2 Particles. *Chem. Mater.* **2003**, *15*, 378–382.
27. Lee, T. L.; Raitano, J. M.; Rennert, O. M.; Chan, S. W.; Chan, W. Y. Accessing the Genomic Effects of Naked Nanoceria in Murine Neuronal Cells. *Nanomedicine* **2012**, *8*, 599–608.
28. Schubert, D.; Dargusch, R.; Raitano, J.; Chan, S. W. Cerium and Yttrium Oxide Nanoparticles Are Neuroprotective. *Biochem. Biophys. Res. Commun.* **2006**, *342*, 86–91.
29. Zhang, H.; He, X.; Zhang, Z.; Zhang, P.; Li, Y.; Ma, Y.; Kuang, Y.; Zhao, Y.; Chai, Z. Nano-CeO_2 Exhibits Adverse Effects at Environmental Relevant Concentrations. *Environ. Sci. Technol.* **2011**, *45*, 3725–3730.
30. Hussain, S.; Al-Nsour, F.; Rice, A. B.; Marshburn, J.; Yingling, B.; Ji, Z.; Zink, J. I.; Walker, N. J.; Garantziotis, S. Cerium Dioxide Nanoparticles Induce Apoptosis and Autophagy in Human Peripheral Blood Monocytes. *ACS Nano* **2012**, *6*, 5820–5829.
31. Suh, W. H.; Suslick, K. S.; Stucky, G. D.; Suh, Y. H. Nanotechnology, Nanotoxicology, and Neuroscience. *Prog. Neurobiol.* **2009**, *87*, 133–170.
32. Tseng, M. T.; Lu, X.; Duan, X.; Hardas, S. S.; Sultana, R.; Wu, P.; Unrine, J. M.; Graham, U.; Butterfield, D. A.; Grulke, E. A.; *et al.* Alteration of Hepatic Structure and Oxidative Stress Induced by Intravenous Nanoceria. *Toxicol. Appl. Pharmacol.* **2012**, *260*, 173–182.
33. Kuchma, M. H.; Komanski, C. B.; Colon, J.; Teblum, A.; Masunov, A. E.; Alvarado, B.; Babu, S.; Seal, S.; Summy, J.; Baker, C. H. Phosphate Ester Hydrolysis of Biologically Relevant Molecules by Cerium Oxide Nanoparticles. *Nanomedicine* **2010**, *6*, 738–744.
34. Deshpande, S.; Patil, S.; Kuchibhatla, S. V. N. T.; Seal, S. Size Dependency Variation in Lattice Parameter and Valency States in Nanocrystalline Cerium Oxide. *Appl. Phys. Lett.* **2005**, *87*, 133113–133116.
35. Taguchi, M.; Takami, S.; Adschiri, T.; Nakane, T.; Sato, K.; Naka, T. Synthesis of Surface-Modified Monoclinic ZrO_2 Nanoparticles Using Supercritical Water. *CrystEngComm* **2012**, *14*, 2132–2138.
36. Nel, A.; Xia, T.; Madler, L.; Li, N. Toxic Potential of Materials at the Nanolevel. *Science* **2006**, *311*, 622–627.
37. Nel, A. E.; Madler, L.; Velegol, D.; Xia, T.; Hoek, E. M.; Somasundaran, P.; Klaessig, F.; Castranova, V.; Thompson, M. Understanding Biophysicochemical Interactions at the Nano-Bio Interface. *Nat. Mater.* **2009**, *8*, 543–557.
38. Rogers, N. J.; Franklin, N. M.; Apte, S. C.; Batley, G. E.; Angel, B. M.; Lead, J. R.; Baalousha, M. Physico-Chemical Behaviour and Algal Toxicity of Nanoparticulate CeO_2 in Freshwater. *Environ. Chem.* **2010**, *7*, 50–60.
39. Yokel, R. A.; Florence, R. L.; Unrine, J. M.; Tseng, M. T.; Graham, U. M.; Wu, P.; Grulke, E. A.; Sultana, R.; Hardas, S. S.; Butterfield, D. A. Biodistribution and Oxidative Stress Effects of a Systemically-Introduced Commercial Ceria Engineered Nanomaterial. *Nanotoxicology* **2009**, *3*, 234–248.
40. Horie, M.; Nishio, K.; Kato, H.; Fujita, K.; Endoh, S.; Nakamura, A.; Miyauchi, A.; Kinugasa, S.; Yamamoto, K.; Niki, E.; *et al.* Cellular Responses Induced by Cerium Oxide Nanoparticles: Induction of Intracellular Calcium Level and Oxidative Stress on Culture Cells. *J. Biochem.* **2011**, *150*, 461–71.
41. Xia, T.; Kovochich, M.; Liong, M.; Madler, L.; Gilbert, B.; Shi, H.; Yeh, J. I.; Zink, J. I.; Nel, A. E. Comparison of the Mechanism of Toxicity of Zinc Oxide and Cerium Oxide Nanoparticles Based on Dissolution and Oxidative Stress Properties. *ACS Nano* **2008**, *2*, 2121–2134.
42. Csordas, G.; Varnai, P.; Golenar, T.; Roy, S.; Purkins, G.; Schneider, T. G.; Balla, T.; Hajnoczky, G. Imaging Interorganelle Contacts and Local Calcium Dynamics at the ER-Mitochondrial Interface. *Mol. Cell* **2010**, *39*, 121–132.
43. Hillegass, J. M.; Shukla, A.; Lathrop, S. A.; MacPherson, M. B.; Fukagawa, N. K.; Mossman, B. T. Assessing Nanotoxicity in Cells *in Vitro*. *Wiley Interdiscip. Rev.: Nanomed. Nanobiotechnol.* **2010**, *2*, 219–231.
44. Sohaebuddin, S.; Thevenot, P.; Baker, D.; Eaton, J.; Tang, L. Nanomaterial Cytotoxicity Is Composition, Size, and Cell Type Dependent. *Part. Fibre Toxicol.* **2010**, *7*, 22.
45. Lee, T. L.; Raitano, J. M.; Rennert, O. M.; Chan, S. W.; Chan, W. Y. Accessing the Genomic Effects of Naked Nanoceria in Murine Neuronal Cells. *Nanomed. Nanotechnol.* **2012**, *8*, 599–608.
46. Yokel, R. A.; Tseng, M. T.; Dan, M.; Unrine, J. M.; Graham, U. M.; Wu, P.; Grulke, E. A. Biodistribution and Biopersistence of Ceria Engineered Nanomaterials: Size Dependence. *Nanomedicine* **2013**, *9*, 398–407.
47. Estevez, A. Y.; Pritchard, S.; Harper, K.; Aston, J. W.; Lynch, A.; Lucky, J. J.; Ludington, J. S.; Chatani, P.; Mosenthal, W. P.; Leiter, J. C.; *et al.* Neuroprotective Mechanisms of Cerium Oxide Nanoparticles in a Mouse Hippocampal Brain Slice Model of Ischemia. *Free Radical Biol. Med.* **2011**, *51*, 1155–1163.
48. Anderson, S. A.; Purich, D. L. A Reinvestigation of Dynein Atpase Kinetics and the Inhibitory-Action of Vanadate. *J. Biol. Chem.* **1982**, *257*, 6656–6658.
49. Lark, E.; Omoto, C. K.; Schumaker, M. F. Functional Multiplicity of Motor Molecules Revealed by a Simple Kinetic-Analysis. *Biophys. J.* **1994**, *67*, 1134–1140.
50. Dell'Orco, D.; Lundqvist, M.; Oslakovic, C.; Cedervall, T.; Linse, S. Modeling the Time Evolution of the Nanoparticle-Protein Corona in a Body Fluid. *PLoS One* **2010**, *5*, e10949.
51. Molinari, M.; Parker, S. C.; Sayle, D. C.; Islam, M. S. Water Adsorption and Its Effect on the Stability of Low Index Stoichiometric and Reduced Surfaces of Ceria. *J. Phys. Chem. C* **2012**, *116*, 7073–7082.
52. Esch, F.; Fabris, S.; Zhou, L.; Montini, T.; Africh, C.; Fornasiero, P.; Comelli, G.; Rosei, R. Electron Localization Determines Defect Formation on Ceria Substrates. *Science* **2005**, *309*, 752–755.
53. Singh, S.; Dosani, T.; Karakoti, A. S.; Kumar, A.; Seal, S.; Self, W. T. A Phosphate-Dependent Shift in Redox State of Cerium Oxide Nanoparticles and Its Effects on Catalytic Properties. *Biomaterials* **2011**, *32*, 6745–6753.
54. Singh, S.; Kumar, A.; Karakoti, A.; Seal, S.; Self, W. T. Unveiling the Mechanism of Uptake and Sub-Cellular Distribution of Cerium Oxide Nanoparticles. *Mol. BioSyst.* **2010**, *6*, 1813–1820.
55. Das, S.; Singh, S.; Dowding, J. M.; Oommen, S.; Kumar, A.; Sayle, T. X.; Saraf, S.; Patra, C. R.; Vlahakis, N. E.; Sayle, D. C.; *et al.* The Induction of Angiogenesis by Cerium Oxide Nanoparticles through the Modulation of Oxygen in Intracellular Environments. *Biomaterials* **2012**, *33*, 7746–7755.
56. Zhang, F.; Jin, Q.; Chan, S.-W. Ceria Nanoparticles: Size, Size Distribution, and Shape. *J. Appl. Phys.* **2004**, *95*, 4319–4326.
57. Cimini, A.; D'Angelo, B.; Das, S.; Gentile, R.; Benedetti, E.; Singh, V.; Monaco, A. M.; Santucci, S.; Seal, S. Antibody-Conjugated PEGylated Cerium Oxide Nanoparticles for Specific Targeting of a Beta Aggregates Modulate Neuronal Survival Pathways. *Acta Biomater.* **2012**, *8*, 2056–2067.
58. Meno, S. R.; Nelson, R.; Hintze, K. J.; Self, W. T. Exposure to Monomethylarsonous Acid (MMA(III)) Leads to Altered Selenoprotein Synthesis in a Primary Human Lung Cell Model. *Toxicol. Appl. Pharmacol.* **2009**, *239*, 130–136.
59. Nandy, B.; Joshi, A.; Ali, Z. S.; Sen, S.; Prasad, N. G. Degree of Adaptive Male Mate Choice Is Positively Correlated with Female Quality Variance. *Sci. Rep.* **2012**, *2*, 447.
60. Trogadas, P.; Parrondo, J.; Ramani, V. CeO_2 Surface Oxygen Vacancy Concentration Governs *In Situ* Free Radical Scavenging Efficacy in Polymer Electrolytes. *ACS Appl. Mater. Interfaces* **2012**, *4*, 5098–6102.
61. Weber, W. H.; Hass, K. C.; McBride, J. R. Raman Study of CeO_2: Second-Order Scattering, Lattice Dynamics, and Particle-Size Effects. *Phys. Rev. B: Condens. Matter* **1993**, *48*, 178–185.
62. Feng, X. D.; Sayle, D. C.; Wang, Z. L.; Paras, M. S.; Santora, B.; Sutorik, A. C.; Sayle, T. X. T.; Yang, Y.; Ding, Y.; Wang, X. D.; *et al.* Converting Ceria Polyhedral Nanoparticles into Single-Crystal Nanospheres. *Science* **2006**, *312*, 1504–1508.
63. Sayle, T. X. T.; Cantoni, M.; Bhatta, U. M.; Parker, S. C.; Hall, S. R.; Mobus, G.; Molinari, M.; Reid, D.; Seal, S.; Sayle, D. C. Strain and Architecture-Tuned Reactivity in Ceria Nanostructures; Enhanced Catalytic Oxidation of CO to CO_2. *Chem. Mater.* **2012**, *24*, 1811–1821.